Deficits in human trisomy 21 iPSCs and neurons

Jason P. Weick[a,1], Dustie L. Held[a], George F. Bonadurer III[a], Matthew E. Doers[a], Yan Liu[a], Chelsie Maguire[a], Aaron Clark[a], Joshua A. Knackert[a], Katharine Molinarolo[a], Michael Musser[a], Lin Yao[a], Yingnan Yin[a], Jianfeng Lu[a], Xiaoqing Zhang[a], Su-Chun Zhang[a,b,c,d], and Anita Bhattacharyya[a,2]

[a]Waisman Center, [b]Neuroscience Training Program, and Departments of [c]Neuroscience and [d]Neurology, School of Medicine and Public Health, University of Wisconsin, Madison, WI 53705

Down syndrome (trisomy 21) is the most common genetic cause of intellectual disability, but the precise molecular mechanisms underlying impaired cognition remain unclear. Elucidation of these mechanisms has been hindered by the lack of a model system that contains full trisomy of chromosome 21 (Ts21) in a human genome that enables normal gene regulation. To overcome this limitation, we created Ts21-induced pluripotent stem cells (iPSCs) from two sets of Ts21 human fibroblasts. One of the fibroblast lines had low level mosaicism for Ts21 and yielded Ts21 iPSCs and an isogenic control that is disomic for human chromosome 21 (HSA21). Differentiation of all Ts21 iPSCs yielded similar numbers of neurons expressing markers characteristic of dorsal forebrain neurons that were functionally similar to controls. Expression profiling of Ts21 iPSCs and their neuronal derivatives revealed changes in HSA21 genes consistent with the presence of 50% more genetic material as well as changes in non-HSA21 genes that suggested compensatory responses to oxidative stress. Ts21 neurons displayed reduced synaptic activity, affecting excitatory and inhibitory synapses equally. Thus, Ts21 iPSCs and neurons display unique developmental defects that are consistent with cognitive deficits in individuals with Down syndrome and may enable discovery of the underlying causes of and treatments for this disorder.

cerebral cortex | developmental disorders

Down syndrome (DS) is the most frequent single cause of human birth defects and intellectual disability (ID) (1). DS is caused by trisomy of chromosome 21 (Ts21) (2), resulting in the triplication of over 400 genes (3–5), which makes elucidation of the precise mechanisms underlying ID in DS a significant challenge. Confounding this difficulty is the relative inaccessibility of human tissue and incomplete human Ts21 in the context of mouse models. Despite these shortcomings, studies using mouse models containing trisomy of parts of syntenic chromosome 21 (HSA21) have put forth several critical hypotheses on the cellular and molecular mechanisms underlying DS features. It is essential, however, to test these hypotheses in human cells with full triplication of HSA21 in a context that allows for normal gene regulation. Here, we used Ts21-induced pluripotent stem cells (iPSCs) to test hypotheses of the underlying causes of ID in DS, with specific regard to neuropathophysiology.

Results

Isogenic Human Ts21 iPSCs. Fibroblasts from two individuals diagnosed with DS were reprogrammed to iPSCs. FISH for HSA21 in one fibroblast line showed mosaicism, where ∼90% of cells carried Ts21, whereas ∼10% were euploid (Fig. 1A). Reprogramming of the mosaic fibroblasts by retrovirus (6) resulted in three viable iPSC clones, two clones that carried Ts21 and one euploid (Fig. 1B). Mosaicism in DS individuals is rare, occurring in ∼1–3% of DS cases (7), but it can also emerge in vitro (8), potentially because of nondisjunction events during cell division. Regardless, the generation of euploid isogenic controls is fortuitous, because they become vital controls for a complex multigene disorder such as DS, potentially limiting the need for multiple iPSC lines to control for genetic and epigenetic variation (9–11). SNP analysis of HSA21 in the euploid DS2U iPSC line ruled out

uniparental disomy (or isodisomy), which is often associated with trisomy rescue (Fig. 1D). Short tandem repeats at various loci indicated that the Ts21 and euploid lines were isogenic other than the presence of Ts21 (Fig. 1E). To increase statistical power, fibroblasts from a second DS individual were reprogrammed using Sendai virus (12), an RNA virus, which yielded another Ts21 iPSC line (Fig. 1C). All iPSC clones were named according to standardized naming procedures (Fig. 1F) (13) and used in all experiments. Importantly, no chromosomal abnormalities, other than Ts21, were observed in any line throughout the duration of this study, in contrast to the propensity of many iPSC lines to acquire aneuploidy (14, 15). Expression of pluripotent genes and proteins POU class 5 homeobox 1 (Oct4), SRY-box containing gene 2 (Sox2), stage-specific embryonic antigen-4 (SSEA-4), and Tra1-81 and lack of expression of the neuroepithelial marker paired box gene 6 (Pax6) (16) and reprogramming genes verified the pluripotency of the iPSCs (Fig. S1 A–D). In addition, all iPSCs expressed markers of each germ layer after nondirected differentiation (Fig. S1).

Theories of the pathophysiology of DS stem from the imbalance of gene expression in critical developmental pathways caused by the presence of an extra HSA21 (17–20). We analyzed global gene expression of DS1 and DS4 Ts21 iPSCs compared with isogenic euploid DS2U to determine if there were gene expression changes that might foreshadow later defects in differentiated tissues. Comparison of gene expression between isogenic cells enabled the identification of changes that were caused by the extra copy of HSA21 and not normal human variation. Both Ts21 iPSC lines (DS1 and DS4) displayed a preferential increase in expression of HSA21 genes compared with genes on other chromosomes (Fig. S2A), consistent with gene expression in Ts21 human ES cells (21). Changes in HSA21 genes seemed evenly distributed across HSA21 (Fig. S2C), and almost 90% were increased (125 of 139) (Dataset S1) with a significantly greater percentage of chromosomal content compared with other chromosomes (Fig. S2A) ($n = 3$, $P < 0.001$). Furthermore, mean fold change for altered genes on HSA21 was significantly greater than all other chromosomes and generally reflected the 3:2 ratio of HSA21 genes (Fig. S2B and Datasets S1 and S2). Together, these data suggest that gene expression in this early pluripotent stage is largely based on simple gene dosage.

Fig. 1. Reprogramming of mosaic fibroblasts yields Ts21 iPSCs and an isogenic control. (*A*) Fibroblast line AG05397 was mosaic for Ts21, with (*Upper*) ~89% of cells carrying three copies [runt-related transcription factor 1 (AML1)/Down syndrome critical region (DSCR); orange], whereas (*Lower*) 10% were disomic for HSA21 (AML1/DSCR; orange). The telomere (TEL) marker (green) was used as a control probe. (*B*) All iPSC lines had morphological characteristics of pluripotent stem cells, and karyotype analysis showed that DS1 and DS4 iPSCs are trisomic, whereas DS2U is disomic for HSA21 (red circles). (*C*) 2DS3 iPSCs from a second DS individual carry Ts21. (*D*) SNP analysis revealed no absence of heterozygosity of HSA21 in the euploid DS2U iPSC line. (*E*) Short terminal repeat analysis revealed that Ts21 and control lines are isogenic at all loci tested. (*F*) Table of different iPSC lines used in this study. (*G*) A heat map shows that genes changed more than fivefold in DS1 and DS4 iPSCs compared with the isogenic DS2U control iPSCs. (*H*) qPCR verification in all Ts21 iPSC lines of various genes that are changed in microarray results. (*I*) Ts21 iPSCs did not exhibit increased oxidative stress compared with their respective controls, which were assayed by DHE. (*J*) The proportion of Ts21 cells that underwent apoptosis was similar to controls, which were assayed by TUNEL+ cells. Error bars represent SEM. (Scale bars: 100 μm.)

Functionally, most of the genes with expression that was changed in Ts21 iPSCs were involved with metabolism, but these changes did not cause changes in proliferation of Ts21 iPSCs (Fig. S1*G*) [Ki67: DS1/4, $P = 0.87$, $n = 4$; 2DS3, $P = 0.4$, $n = 3$; phospho-histone H3 (PHH3): DS1/4, $P = 0.90$, $n = 4$; 2DS3, $P = 0.07$, $n = 3$]. Some of the largest expression changes in Ts21 iPSCs were in non-HSA21 genes involved in transcriptional activation and the response to oxidative stress (OS; e.g., catalase, *CAT*) (Fig. 1 *G* and *H*). Similar expression changes were detected in Ts21 neurons (see below). Many of the highly up-regulated transcription factors are members of the zinc finger family that regulate the expression of a variety of downstream genes and have been implicated in numerous developmental disorders affecting different

cell lineages (22). Based on the increased expression of OS responsive genes in Ts21 iPSCs, we evaluated the cells for evidence of OS but found no increase in OS, which was assayed by dihydroethidium (DHE) (Fig. 1*I*) (DS1, $P = 0.62$; DS4, $P = 0.98$; 2DS3, $P = 0.95$; $n = 2$ each), or cell death in Ts21 iPSCs compared with their control counterparts (Fig. 1*J*) (DS1, $P = 0.79$, $n = 3$; DS4, $P = 0.86$, $n = 2$; 2DS3, $P = 0.57$, $n = 2$).

Generation of Early-Born Cortical Neurons Is Not Affected by Ts21. A universal characteristic of DS is the presence of mild to moderate cognitive impairment, potentially because of diminished cortical neuron numbers in DS brains (23–26). However, using our established protocol for cortical neuronal differentiation (27,

Fig. 2. Generation of cortical neurons is not affected by Ts21. (*A*) FACS analysis reveals no difference in the propensity of Ts21 iPSCs to generate *Pax6*⁺ neuroepithelia. (*B*) Ts21 iPSC-derived neural progenitor cells exhibited increases in many HSA21 and oxidative stress genes, which were assayed by qPCR. (*C*) Transcript expression of dorsal telencephalic markers was evident in neurons differentiated from all lines, but ventral forebrain [NK2 homeobox 1 (*Nkx2.1*)], hindbrain [gastrulation brain homeobox 2 (*Gbx2*)], and spinal cord [homeobox B4 (*Hoxb4*)] markers were not readily observed. (*D* and *E*) Immunostaining of cultured cells shows no difference in β$_{III}$-tubulin⁺ neurons or forebrain markers [forkhead box G1 (*FoxG1*) and orthodenticle homeobox 2 (*OTX2*)] across iPSC lines. (*F*) Heat map depicts global gene expression changes more than threefold in isogenic Ts21 (DS1 and DS4) vs. control (DS2U) iPSC-derived neuronal cultures. (*G*) qPCR verification of various genes up-regulated in microarray results in all iPSC-derived neuronal cultures. (*H*) DS neurons exhibited increased oxidative stress, which was assayed by DHE, and (*I*) mitochondrial membrane potential. (*J*) The proportion of Ts21 cells that underwent apoptosis was similar to controls, which were assayed by TUNEL⁺ cells. (Scale bars: 50 μm.) Error bars represent SEM. *$P < 0.05$. (*A*, *B*, *D*, *E*, and *J*) For measures where no significant differences were found between groups, dashed lines indicate the average of the control groups (DS2U and IMR90).

28), we found that all iPSC lines robustly differentiated to *Pax6*⁺ neuroepithelia by day 10 (16) (Fig. 2*A*), consistent with the best efficiency shown by other iPSC lines (11). Neural progenitors differentiated from Ts21 iPSCs also had increased catalase expression, similar to Ts21 iPSCs, but expressed other HSA21 genes implicated in OS at the expected 1.5-fold (Fig. 2*B*). PCR analysis and immunostaining revealed no difference in the regional identity of β$_{III}$-tubulin⁺ neurons in euploid and Ts21 cultures, where the vast majority expressed dorsal forebrain markers (Fig. 2*C*). Similarly, quantification of β$_{III}$-tubulin⁺ neurons at 6 wk of differentiation revealed no significant differences between the fraction of neurons in euploid and Ts21 cultures (Fig. 2 *D* and *E*) (β$_{III}$-tubulin: $n = 6$, $P = 0.78$; *FoxG1*: $n = 6$, $P = 0.88$; *Otx2*: $n = 6$, $P = 0.29$).

Thus, although studies in both human and mouse have implicated reduced cortical neurogenesis (24, 29–33), our data

suggest that early cortical neural progenitors and initial waves of differentiating neurons are unaffected in the presence of Ts21. The reported reductions in cortical neurons in DS brains may affect primarily late-born neurons that are not being evaluated in our study (24, 30, 34, 35).

Gene Expression Changes and Oxidative Stress Vulnerability. To gain insight into the neuropathophysiology of Ts21 neurons, we analyzed global gene expression of 30-d-old neurons from DS1 and DS4 Ts21 iPSCs compared with those neurons from euploid DS2U iPSCs (Fig. 2*F*). Ts21 neurons displayed a preferential increase in expression of HSA21 genes, similar to Ts21 iPSCs in number and chromosomal distribution (Fig. S2 *D–F*). Virtually all of the HSA21 genes with expression that was changed in Ts21 neurons were increased (112 of 113) (Dataset S3), a significantly greater percentage of chromosomal content compared with

other chromosomes (Fig. S2D). Furthermore, mean fold change for altered genes on HSA21 was significantly greater than all other chromosomes and generally reflected the 3:2 ratio of HSA21 genes (Fig. S2E and Dataset S4).

A central tenet in DS research is that symptoms are caused by modest increases in expression of trisomic genes and that these expression changes, in turn, cause dysregulation of normal cellular function through alterations in signaling pathways. Our data in both Ts21 iPSCs and neurons largely agree with this principle, whereby gene expression changes were based on gene dosage, but the greatest changes in Ts21 cells were observed for genes on chromosomes other than 21 (Figs. 1G and 2F and Datasets S2 and S4). The largest gene expression changes (more than fivefold) in both Ts21 iPSCs and neurons were of genes associated with transcriptional regulation and OS that we confirmed by quantitative PCR (qPCR) from all Ts21 lines (Figs. 1 G and H and 2 F and G). We did not observe expression of superoxide dismutase 1 (SOD1) and amyloid precursor protein (APP), HSA21 genes known to be involved in OS over the expected amount of 1.5-fold (Figs. 1H and 2G), but these modest increases may be sufficient to drive the response to OS. Ts21 neurons did exhibit increased OS, which was assayed by DHE (Fig. 2H) (DS1/4, $P = 0.005$; 2DS3, $P = 0.03$; $n = 3$ each). Furthermore, the increased expression of v-ets erythroblastosis virus E26 oncogene homolog 2 (ETS2), an HSA21-encoded transcription factor implicated in neuronal death and mitochondrial dysfunction (36), over the expected 1.5-fold in Ts21 neurons (Fig. 2G) prompted us to assess mitochondrial health in these cells. We

detected increased mitochondrial membrane potential, a feature reported in human Ts21 neurons (37, 38) (Fig. 2I) (DS1, $P = 0.04$; 2DS3, $P = 0.01$; $n = 2$ each). However, we did not detect a significant increase in cell death in Ts21 neurons (Fig. 2J) (DS1, $P = 0.62$; 2DS3, $P = 0.94$; $n = 2$ each).

DS Neurons Are Deficient in Their Ability to Form Functional Synapses.
Changes in neuronal excitability and synaptic efficacy have been shown to contribute to cognitive impairment in DS mouse models (33, 39, 40). Whole-cell patch clamp recordings were performed on Ts21 iPSC-derived neurons between 5 and 6 wk, a time when human PSC-derived neurons have substantial synaptic activity (41, 42). Results revealed equivalent mean inward sodium and outward potassium currents in response to voltage steps as well as action potential (AP) generation in response to depolarizing current injections (Fig. 3 A and B) (Na$^+$ current: DS1: $P = 0.33$; DS4: $P = 0.37$; 2DS3: $P = 0.29$; K$^+$ current: DS1: $P = 0.18$; DS4: $P = 0.11$; 2DS3: $P = 0.97$; $n = 6$ replicates with ~90 total cells/group) (SI Materials and Methods). Furthermore, no differences were seen in multiple physiological parameters, including cell size (capacitance), resting membrane potential, and AP amplitude in response to current injections (Fig. S3A), suggesting that basic physiological properties are unchanged in Ts21 iPSC-derived neurons at early stages. Interestingly, we found trends in all groups and significant reductions in most groups in the fraction of Ts21 iPSC-derived neurons that displayed spontaneous postsynaptic currents (sPSCs) (Fig. 3D) (DS1: $P = 0.04$; DS4: $P = 0.01$; 2DS3: $P = 0.06$; $n = 6$ each) as well as the sPSC frequency in Ts21 cells compared with
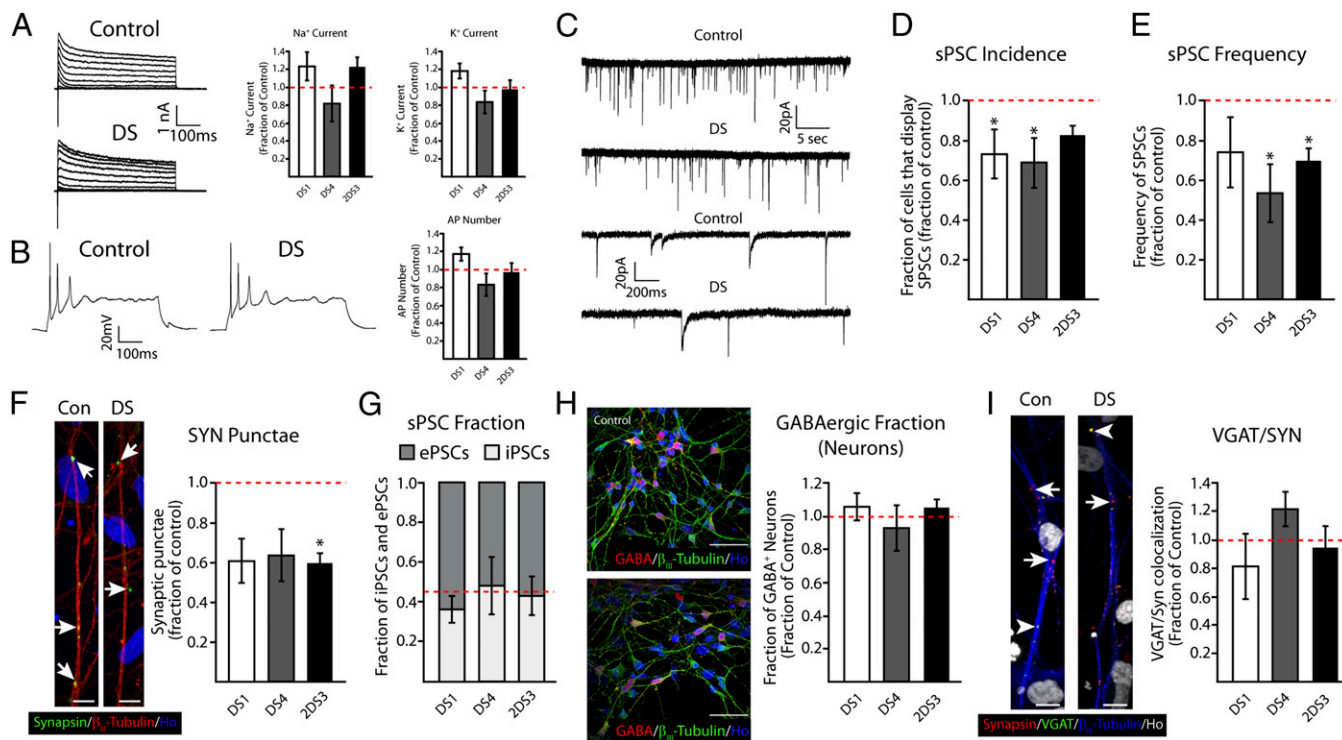
Fig. 3. Forebrain Ts21 neurons display synaptic deficits across transmitter phenotype. (A and B) Representative whole-cell patch clamp traces illustrate that Ts21 (DS) did not show differences in (A) sodium (Na$^+$) and potassium (K$^+$) currents or (B) the number of APs in response to current injection. (C) Representative voltage clamp (−70 mV) traces show that both control and DS neurons displayed sPSCs. Expanded timescale (traces 3 and 4) illustrates sPSCs with different kinetics in both control and DS neurons. (D) Significantly fewer DS neurons display synaptic activity relative to controls (DS2U: 86 ± 3.9%; IMR90: 81 ± 3.2%). (E) DS neurons also displayed significantly lower frequencies of sPSCs compared with controls (DS2U: 0.48 Hz; IMR90: 0.92 Hz). (F) Representative images of control and DS β$_{III}$-tubulin$^+$ neurites (red) displaying synapsin$^+$ puncta (green; arrows). (Blue) Hoechst. Pooled data revealed fewer synapsin$^+$ puncta in DS neurons compared with controls (DS2U: 2.9 ± 0.6/100 μm; IMR90: 4.4 ± 0.6/100 μm). (G) The proportion of excitatory and inhibitory sPSCs was not changed in DS cultures relative to controls [excitatory PSCs (ePSCs): DS2U: 0.54 ± 0.07 Hz; IMR90: 0.55 ± 0.11 Hz; iPSCs: DS2U: 0.46 ± 0.06 Hz; IMR90: 0.45 ± 0.09 Hz]. No differences were observed in (H) the fraction of GABA$^+$ neurons compared with controls (DS2U: 47.7 ± 1.9%; IMR90: 46.2 ± 2.2%) or (I) the fraction of VGAT$^+$/synapsin$^+$ puncta (arrowheads) in DS cultures compared with controls (DS2U: 37.1 ± 6.1%; IMR90: 41.5 ± 4.5%). Error bars represent SEM. *$P < 0.05$. (Scale bars: F and I, 10 μm; H, 50 μm.)

NEUROSCIENCE

euploid controls (Fig. 3 C–E) (DS1: P = 0.16; DS4: P = 0.04; 2DS3: P = 0.04; n = 6 each). This reduction was mirrored by a decrease in the number of synapsin[+] punctae on Ts21 neurites (Fig. 3F and *SI Materials and Methods*) (DS1: P = 0.09; DS4: P = 0.17; 2DS3: P = 0.04; n = 3 replicates with ∼200 total neurites/group).

Studies in DS mouse models have shown impaired synaptic efficacy because of increased inhibition (40, 43), which is potentially caused by overproduction of inhibitory interneurons at the expense of glutamatergic projection neurons (44). However, we found no significant difference in the ratio of excitatory to inhibitory sPSCs (Fig. 3G) (DS1: P = 0.38; DS4: P = 0.83; 2DS3: P = 0.86; n = 6 each), the percentage of neurons that expressed GABA (Fig. 3H) (DS1: P = 0.59; DS4: P = 0.94; 2DS3: P = 0.52; n = 3 each), or the fraction of synapses that stained positive for vesicular GABA transporter (VGAT) (Fig. 3I) (DS1: P = 0.50; DS4: P = 0.96; 2DS3: P = 0.77; n = 3 each). Importantly, the biophysical properties (e.g., amplitude, rise time, and decay constant) of sPSCs did not differ between groups (Fig. S3 C–E), and the proportion of cells that displayed AP firing (Fig. S3A) as well as spontaneous AP frequency (Fig. S3F) remained unchanged between groups. Together, these data suggest that changes in overall excitability of human Ts21 iPSC-derived neurons did not cause reductions in synaptic activity.

Discussion

Although DS is the most common genetic cause of intellectual disability and its etiology has been known for over 50 y (2), its underlying mechanisms and effective treatments have yet to be discovered. Here, Ts21 iPSCs and their neuronal derivatives displayed a combination of predictable and unique changes in gene expression as well as a distinct physiological phenotype in forebrain neurons. Although these two phenotypes, susceptibility to oxidative stress and reduced synaptic activity, may be related (45, 46), we will examine them independently, because the current data do not address any mechanistic connection.

Gene Expression Changes Implicate Oxidative Stress Vulnerability. Global gene expression analysis of both Ts21 iPSCs and forebrain neurons revealed changes in HSA21 genes consistent with gene dosage, suggesting a generally passive epigenetic regulatory process in these cells. Interestingly, dramatic changes were observed in a relatively small number of non-HSA21 genes that were largely maintained during the switch from pluripotent to differentiated cells. These genes included those that encode transcription factors belonging to the zinc finger family, many of which remain uncharacterized. Furthermore, expression of genes that are involved in the response to OS was significantly up-regulated in Ts21 cells. The striking overexpression of catalase, an indicator of a cell's response to OS, in Ts21 cells may be an early sign of the sensitivity to OS that these cells, particularly neurons, display (47). However, we did not see a significant increase in cell death in DS iPSCs or neurons, suggesting that OS gene up-regulation may act as a compensatory mechanism to allow survival of Ts21 cells, consistent with previous studies using exogenous catalase (47). OS was detectable in Ts21 differentiated neuronal cultures but not Ts21 iPSCs. Therefore, a unique mechanism may be in play in Ts21 cells during early developmental stages, where compensatory changes in OS genes allow for nearly normal cell proliferation and differentiation but cells remain highly susceptible to insults later in development (38, 47–50). This mechanism may exacerbate the consequences of *APP* overexpression that predispose DS individuals to develop Alzheimer's disease pathology (51–54).

DS iPSC-Derived Neurons Display a Significant Synaptic Deficit. Recent studies in DS mouse models have put forth the hypothesis that an imbalance in the excitation–inhibition ratio may underlie ID in DS. Results have shown impaired synaptic efficacy because of increased inhibition in various brain regions (40, 43),

potentially caused by overproduction of inhibitory interneurons that primarily originate from the ventral forebrain, at the expense of glutamatergic projection neurons (44). Synaptic deficits in humans have been inferred from ultrastructural studies showing abnormal dendritic spine morphology (23, 55, 56). Our results reveal unaltered glutamatergic and GABAergic neuronal populations during early cortical neuronal differentiation. We show that, although many neuronal characteristics appear normal, Ts21 iPSC-derived neurons display a significant synaptic deficit that is present in both glutamatergic and GABAergic subtypes. Recently, the work by Shi et al. (57) reported "normal" synaptic activity in glutamatergic neurons differentiated from a single Ts21 iPSC line. However, the absence of GABAergic neurons in their system and diminutive excitatory synaptic currents (<5 pA) suggest aberrant network formation as well. Although previous studies and current therapeutic strategies target an imbalanced excitation–inhibition ratio as a primary cause of learning and memory deficits, these data suggest that early Ts21 forebrain neurons are deficient in their ability to form functional synapses, generating a quieter network as a whole. Therefore, current therapeutic strategies aimed at excitation–inhibition imbalance may have different effects in individuals with DS than DS mouse models.

It is important to note, however, that a direct comparison between these data and the data of mature mouse models should be approached with caution. The imbalance in the excitation–inhibition ratio in mouse models reflects the summation of synaptic activities of many neuronal types, including late-born interneurons. Nonetheless, our study reveals synaptic deficits, even in early-born projection neurons.

Future studies of iPSC-derived neuronal maturation, when new neurons (particularly interneurons originating from the ventral forebrain) are added to neural networks, will assist in the interpretation of stem cell-based assays and their synthesis with rodent studies. The examination of the role of Ts21 astrocytes in neuronal maturation and synaptogenesis is also crucial. In addition, it will be important to test hypotheses of premature death in DS neurons by determining whether Ts21 iPSC-derived human neurons die with long-term culture, which has been shown for human Ts21 neurons cultured from fetal neural progenitor cells (47).

Together, these results reveal predicted features of DS cells and identify deficits that may influence mechanistic studies, small-molecule screening, and genetic manipulation to identify therapeutic targets for this common but understudied disorder.

Materials and Methods

Reprogramming. Fibroblast lines AG05397 and GM02504 were obtained from the Coriell Institute for Medical Research. Fibroblasts were reprogrammed to iPSCs according to previously published methods (6, 12). The isogenic clone was unaffected (U), meaning that it does not carry a third copy of HSA21. Karyotype analysis (G banding and FISH), short tandem repeat confirmation, and SNP analysis were carried out at WiCell Research Institute using standard protocols.

iPSC Culture and Differentiation. Three Ts21 iPSC lines (DS1, DS4, and 2DS3) and two euploid iPSC lines (DS2U and IMR90-4) (58) were used in each experiment in this study. iPSCs were maintained and differentiated according to previously established methods (59–61) (*SI Materials and Methods*, Table S1).

Gene Expression Analysis. Three independent RNA samples were collected from the isogenic Ts21 and control iPSCs (DS1, DS4, and DS2U) between passages 24 and 48 and from day 30 neurons. All samples were compared with Universal Human Reference RNA (Stratagene). RNA amplification, fluorescent labeling, array hybridization, scanning, scoring, and cataloging online were performed by the University of Wisconsin at Madison Biotechnology Center using Affymetrix human U133 Plus 2.0 gene chips. Statistical analyses of the microarray data were carried out using Genesifter software (Geospiza). Student t tests were conducted for each dataset, with only genes with a P value < 0.05 being considered in the statistical analysis. Subsequent analyses used one-way ANOVA followed by Tukey honestly significant difference (HSD) posthoc tests. Data sharing is accomplished by deposition of the data into the Gene Expression Omnibus, a public functional genomics data repository supporting minimum information about a microarray

experiment (MIAME)-compliant data submissions (http://www.ncbi.nlm.nih.gov/geo/). qPCR validation of changed genes was carried out on all lines.

Oxidative Stress Assays. Oxidative stress was measured using DHE (Life Technologies). Mitochondrial membrane potential was assayed using membrane-permeable JC-1 dye (Cayman Chemical).

Electrophysiological Recordings. Whole-cell patch clamp recordings were performed on paired, age-matched populations of Ts21 and control cells after 5 and 6 wk of differentiation (n = 9 independent paired experiments) (*SI Materials and Methods*).

1. Parker SE, et al. (2010) Updated National Birth Prevalence estimates for selected birth defects in the United States, 2004–2006. *Birth Defects Res A Clin Mol Teratol* 88(12):1008–1016.
2. Lejeune J, Turpin R, Gautier M (1959) Le mongolisme, premier exemple d'aberration autosomique humaine. *Annals of Genetics* 1(2):41–49.
3. Gardiner K, Davisson M (2000) The sequence of human chromosome 21 and implications for research into Down syndrome. *Genome Biol* 1(2):REVIEWS0002.
4. Sturgeon X, Gardiner KJ (2011) Transcript catalogs of human chromosome 21 and orthologous chimpanzee and mouse regions. *Mamm Genome* 22(5–6):261–271.
5. Letourneau A, Antonarakis SE (2012) Genomic determinants in the phenotypic variability of Down syndrome. *Prog Brain Res* 197(2012):15–28.
6. Takahashi K, et al. (2007) Induction of pluripotent stem cells from adult human fibroblasts by defined factors. *Cell* 131(5):861–872.
7. Devlin L, Morrison PJ (2004) Mosaic Down's syndrome prevalence in a complete population study. *Arch Dis Child* 89(12):1177–1178.
8. Maclean GA, et al. (2012) Altered hematopoiesis in trisomy 21 as revealed through in vitro differentiation of isogenic human pluripotent cells. *Proc Natl Acad Sci USA* 109(43):17567–17572.
9. Bock C, et al. (2011) Reference Maps of human ES and iPS cell variation enable high-throughput characterization of pluripotent cell lines. *Cell* 144(3):439–452.
10. Guenther MG, et al. (2010) Chromatin structure and gene expression programs of human embryonic and induced pluripotent stem cells. *Cell Stem Cell* 7(2):249–257.
11. Hu BY, et al. (2010) Neural differentiation of human induced pluripotent stem cells follows developmental principles but with variable potency. *Proc Natl Acad Sci USA* 107(9):4335–4340.
12. Seki T, et al. (2010) Generation of induced pluripotent stem cells from human terminally differentiated circulating T cells. *Cell Stem Cell* 7(1):11–14.
13. Luong MX, et al. (2011) A call for standardized naming and reporting of human ESC and iPSC lines. *Cell Stem Cell* 8(4):357–359.
14. Boulting GL, et al. (2011) A functionally characterized test set of human induced pluripotent stem cells. *Nat Biotechnol* 29(3):279–286.
15. Mayshar Y, et al. (2010) Identification and classification of chromosomal aberrations in human induced pluripotent stem cells. *Cell Stem Cell* 7(4):521–531.
16. Zhang X, et al. (2010) Pax6 is a human neuroectoderm cell fate determinant. *Cell Stem Cell* 7(1):90–100.
17. Reeves RH, Baxter LL, Richtsmeier JT (2001) Too much of a good thing: Mechanisms of gene action in Down syndrome. *Trends Genet* 17(2):83–88.
18. Gardiner K, et al. (2010) Down syndrome: From understanding the neurobiology to therapy. *J Neurosci* 30(45):14943–14945.
19. Epstein CJ (1990) The consequences of chromosome imbalance. *Am J Med Genet Suppl* 7(1990):31–37.
20. Antonarakis SE (2001) Chromosome 21: From sequence to applications. *Curr Opin Genet Dev* 11(3):241–246.
21. Biancotti JC, et al. (2010) Human embryonic stem cells as models for aneuploid chromosomal syndromes. *Stem Cells* 28(9):1530–1540.
22. Hui CC, Angers S (2011) Gli proteins in development and disease. *Annu Rev Cell Dev Biol* 27:513–537.
23. Wisniewski KE, Laure-Kamionowska M, Wisniewski HM (1984) Evidence of arrest of neurogenesis and synaptogenesis in brains of patients with Down's syndrome. *N Engl J Med* 311(18):1187–1188.
24. Ross MH, Galaburda AM, Kemper TL (1984) Down's syndrome: Is there a decreased population of neurons? *Neurology* 34(7):909–916.
25. Larsen KB, et al. (2008) Reduced cell number in the neocortical part of the human fetal brain in Down syndrome. *Ann Anat* 190(5):421–427.
26. Golden JA, Hyman BT (1994) Development of the superior temporal neocortex is anomalous in trisomy 21. *J Neuropathol Exp Neurol* 53(5):513–520.
27. Li XJ, et al. (2009) Coordination of sonic hedgehog and Wnt signaling determines ventral and dorsal telencephalic neuron types from human embryonic stem cells. *Development* 136(23):4055–4063.
28. Pankratz MT, et al. (2007) Directed Neural Differentiation of hESCs via an Obligated Primitive Anterior Stage. *Stem Cells* 25(6):1511–1520.
29. Wisniewski KE (1990) Down syndrome children often have brain with maturation delay, retardation of growth, and cortical dysgenesis. *Am J Med Genet Suppl* 7(1990):274–281.
30. Schmidt-Sidor B, Wisniewski KE, Shepard TH, Sersen EA (1990) Brain growth in Down syndrome subjects 15 to 22 weeks of gestational age and birth to 60 months. *Clin Neuropathol* 9(4):181–190.
31. Haydar TF, Nowakowski RS, Yarowsky PJ, Krueger BK (2000) Role of founder cell deficit and delayed neuronogenesis in the microencephaly of the trisomy 16 mouse. *J Neurosci* 20(11):4156–4164.
32. Colon EJ (1972) The structure of the cerebral cortex in Down's Syndrome: A quantitative analysis. *Neuropädiatrie* 3(4):362–376.
33. Chakrabarti L, Galdzicki Z, Haydar TF (2007) Defects in embryonic neurogenesis and initial synapse formation in the forebrain of the Ts65Dn mouse model of Down syndrome. *J Neurosci* 27(43):11483–11495.
34. Bhattacharyya A, Svendsen CN (2003) Human neural stem cells: A new tool for studying cortical development in Down's syndrome. *Genes Brain Behav* 2(3):179–186.
35. Bhattacharyya A, McMillan E, Chen SI, Wallace K, Svendsen CN (2009) A critical period in cortical interneuron neurogenesis in down syndrome revealed by human neural progenitor cells. *Dev Neurosci* 31(6):497–510.
36. Helguera P, et al. (2005) ets-2 promotes the activation of a mitochondrial death pathway in Down's syndrome neurons. *J Neurosci* 25(9):2295–2303.
37. Busciglio J, et al. (2002) Altered metabolism of the amyloid beta precursor protein is associated with mitochondrial dysfunction in Down's syndrome. *Neuron* 33(5):677–688.
38. Helguera P, et al. (2013) Adaptive downregulation of mitochondrial function in down syndrome. *Cell Metab* 17(1):132–140.
39. Belichenko PV, Kleschevnikov AM, Salehi A, Epstein CJ, Mobley WC (2007) Synaptic and cognitive abnormalities in mouse models of Down syndrome: Exploring genotype-phenotype relationships. *J Comp Neurol* 504(4):329–345.
40. Kleschevnikov AM, et al. (2004) Hippocampal long-term potentiation suppressed by increased inhibition in the Ts65Dn mouse, a genetic model of Down syndrome. *J Neurosci* 24(37):8153–8160.
41. Wu H, et al. (2007) Integrative genomic and functional analyses reveal neuronal subtype differentiation bias in human embryonic stem cell lines. *Proc Natl Acad Sci USA* 104(34):13821–13826.
42. Weick JP, Liu Y, Zhang SC (2011) Human embryonic stem cell-derived neurons adopt and regulate the activity of an established neural network. *Proc Natl Acad Sci USA* 108(50):20189–20194.
43. Fernandez F, Garner CC (2007) Over-inhibition: A model for developmental intellectual disability. *Trends Neurosci* 30(10):497–503.
44. Chakrabarti L, et al. (2010) Olig1 and Olig2 triplication causes developmental brain defects in Down syndrome. *Nat Neurosci* 13(8):927–934.
45. Wang Y, Floor E (1998) Hydrogen peroxide inhibits the vacuolar H+-ATPase in brain synaptic vesicles at micromolar concentrations. *J Neurochem* 70(2):646–652.
46. Chen BT, Avshalumov MV, Rice ME (2001) H(2)O(2) is a novel, endogenous modulator of synaptic dopamine release. *J Neurophysiol* 85(6):2468–2476.
47. Busciglio J, Yankner BA (1995) Apoptosis and increased generation of reactive oxygen species in Down's syndrome neurons in vitro. *Nature* 378(6559):776–779.
48. Esposito G, et al. (2008) Genomic and functional profiling of human Down syndrome neural progenitors implicates S100B and aquaporin 4 in cell injury. *Hum Mol Genet* 17(3):440–457.
49. Coskun PE, Busciglio J (2012) Oxidative stress and mitochondrial dysfunction in Down's syndrome: Relevance to aging and dementia. *Curr Gerontol Geriatr Res* 2012(2012):383170.
50. Briggs JA, et al. (2013) Integration-free induced pluripotent stem cells model genetic and neural developmental features of down syndrome etiology. *Stem Cells* 31(3):467–478.
51. Zigman WB, Lott IT (2007) Alzheimer's disease in Down syndrome: Neurobiology and risk. *Ment Retard Dev Disabil Res Rev* 13(3):237–246.
52. Zhu X, Lee HG, Perry G, Smith MA (2007) Alzheimer disease, the two-hit hypothesis: An update. *Biochim Biophys Acta* 1772(4):494–502.
53. Zana M, Janka Z, Kálmán J (2007) Oxidative stress: A bridge between Down's syndrome and Alzheimer's disease. *Neurobiol Aging* 28(5):648–676.
54. Perluigi M, Butterfield DA (2012) Oxidative stress and Down syndrome: A route toward Alzheimer-like dementia. *Curr Gerontol Geriatr Res* 2012(2012):724904.
55. Weitzdoerfer R, Dierssen M, Fountoulakis M, Lubec G (2001) Fetal life in Down syndrome starts with normal neuronal density but impaired dendritic spines and synaptosomal structure. *J Neural Transm Suppl* 61(2001):59–70.
56. Takashima S, Becker LE, Armstrong DL, Chan F (1981) Abnormal neuronal development in the visual cortex of the human fetus and infant with down's syndrome. A quantitative and qualitative Golgi study. *Brain Res* 225(1):1–21.
57. Shi Y, et al. (2012) A human stem cell model of early Alzheimer's disease pathology in Down syndrome. *Sci Transl Med* 4(124):124ra29.
58. Yu J, et al. (2007) Induced pluripotent stem cell lines derived from human somatic cells. *Science* 318(5858):1917–1920.
59. Hu BY, Zhang SC (2010) Directed differentiation of neural-stem cells and subtype-specific neurons from hESCs. *Methods Mol Biol* 636(2010):123–137.
60. Zhang SC, Wernig M, Duncan ID, Brüstle O, Thomson JA (2001) In vitro differentiation of transplantable neural precursors from human embryonic stem cells. *Nat Biotechnol* 19(12):1129–1133.
61. Zhang SC (2006) Neural subtype specification from embryonic stem cells. *Brain Pathol* 16(2):132–142.

NEUROSCIENCE

Weick et al.

Supporting Information

SI Materials and Methods

Induced Pluripotent Stem Cell Culture and Differentiation. Induced pluripotent stem cells (iPSCs) were maintained and differentiated according to previously established methods (1–4). After separation from feeder cells and maintenance in suspension culture for 7 d, aggregates of human iPSCs were differentiated to primitive neuroepithelial aggregates (NEAs) in an adherent culture in neural induction medium consisting of DMEM/F12 (Invitrogen), N2 supplement (1:100; Invitrogen), and heparin (2 µg/mL; Sigma). NEAs were mechanically detached at day 14 and cultured in suspension in neural induction medium with B27 supplement (1:100; Invitrogen). For neuronal differentiation, four to six NEAs were grown on polyornithine/laminin-coated coverslips in neural differentiation medium containing DMEM/F12, N2 (1:50), B27 (1:100), 10 ng/mL brain derived neurotrophic factor (BDNF) (Peprotech), 10 ng/mL glial derived neurotrophic factor (GDNF) (R&D Systems), cAMP (Sigma), and ascorbic acid (Sigma). For three-germ layer analysis, embryoid bodies generated from iPSCs were maintained in suspension in human embryonic stem cell (hESC) media (without FGF2) for at least 30 d and up to 6 wk.

RT-PCR and Quantitative RT-PCR. RNA was isolated from cells using the E.Z.N.A. Total RNA Kit I (Omega Bio-Tek) and reverse transcribed to cDNA using the qScript cDNA SuperMix (Quanta Biosciences). PCR reactions containing 2XGoTaq Green Master Mix (Promega), 1 µM forward and reverse primers, 5 ng cDNA, and water were amplified using a G-Storm thermocycler. PCR products were resolved on a 2% (vol/vol) agarose gel and visualized using ethidium bromide under UV light. Quantitative PCR reactions were performed in triplicate with SYBR Green PCR Master Mix (Applied Biosystems) and run on an Applied Biosystems 7500 Real-Time PCR System; β-actin was used to normalize gene expression between runs and cell lines unless otherwise listed. Analysis of results was performed using the comparative C_T method to determine fold change for a given primer (5).

Immunofluorescence. Cells were fixed in 4% paraformaldehyde in PBS for 15 min and subsequently stored in PBS. Cells were permeabilized and blocked for 30 min in 5% serum and 0.2% Triton X-100 before being incubated in the primary antibody and 5% serum at 4 °C overnight. Cells were subsequently washed and stained with Alexa Fluor (Invitrogen) secondary antibodies in 5% serum for 30 min before being washed and dyed with Hoechst for 5 min and mounted to glass slides with Fluoromount-G Mounting Media (Beckman Coulter).

Cell Death Assay. Cell death was assessed with the TUNEL assay (Promega) according to the manufacturer's directions. Cells on coverslips were imaged using a fluorescence microscope at 20×, and the images were evaluated using Elements software (Nikon Instruments). Total nuclei (~500) that underwent apoptosis were quantified.

Cellular Assays. Oxidative stress in live cells was measured using dihydroethidium (5 µm; Invitrogen). Dihydroethidium (DHE) was added directly to culture medium. Cells were incubated for 30 min, washed one time with PBS, and fixed in 4% paraformaldehyde (20 min) followed by Hoechst and mounting. Fluorescent intensity was measured using Nikon Elements, and the intensity of trisomy of chromosome 21 (Ts21) cells was compared with their respective control cells. Mitochondrial membrane potential was assessed on live cells using the membrane-permeable dye JC-1 (Cayman Chemical). JC-1 was added directly to culture medium (1:20) and imaged using the Biostation-IM Live Cell Recorder (Nikon Instruments). The ratio of GFP (green) to mCherry (red) fluorescence was calculated using the Biostation software, and ratios of Ts21 cells were compared with their respective controls.

Flow Cytometry. Cells were harvested with 0.5% trypsin-EDTA, fixed in 0.1% paraformaldehyde, and permeabilized in 90% methanol before being filtered through a 70-µm cell strainer. The dissociated cells were resuspended in FACS buffer that was comprised of PBS, 2% donkey serum, and 0.01% NaN₃. Cells were incubated overnight at 4 °C with primary antibodies or normal mouse IgG as a control followed by washing and staining with secondary antibodies for 1 h (6). Samples were analyzed with an FACSCalibur (BD Biosciences) running FlowJo software (Treestar).

Synaptic Density. Six-week-old iPSC-derived neurons were labeled with antisynapsin-1, antivesicular GABA transporter (VGAT), $β_{III}$-tubulin (Table S1), and Hoechst nuclear stain (Invitrogen). Neurons were imaged using a Nikon C1 Confocal Microscope running Nikon EZ-C1 software (v.3.5; Nikon Instruments). Four-color images were separated by channel and counted using Metamorph software (Molecular Devices). Regions of interest along randomly selected $β_{III}$-tubulin⁺ neurites were manually traced and transferred to synapsin-1 images for counting. Independent thresholds were set per replicate for synapsin-1 images and applied equally across conditions. A total of seven neurites were analyzed per image, with 10–12 images analyzed per condition (control vs. Ts21) in each of a minimum of three replicates per time point (i.e., three independent differentiated cultures). Therefore, the approximate numbers of neurites per condition = 7 neurites × 10 images × 3 cultures ~ 210 neurites/condition). For VGAT/synapsin analysis, punctae for each were counted separately using independent thresholds and then merged to determine colocalization percentage. The synaptic density of control neurons was pooled, and the density of Ts21 neurons was compared with this pooled value to determine the fraction of control. All *n* values for immunocytochemical analyses represent independent cellular differentiation experiments.

Gene Expression Analysis. Three independent RNA samples were collected from Down syndrome (DS) and control iPSCs between passages 24 and 48 and from day 30 neurons. All samples were compared with Universal Human Reference RNA (Stratagene). RNA amplification, fluorescent labeling, array hybridization, scanning, scoring, and cataloging online were performed by the University of Wisconsin at Madison Biotechnology Center using Affymetrix human U133 Plus 2.0 gene chips; *t* tests were performed using Genesifter software (Geospiza) to generate gene lists (Datasets S1–S4). Subsequent analyses used one-way ANOVA followed by Tukey honestly significant difference (HSD) posthoc tests. Data sharing is accomplished by deposition of the data into the Gene Expression Omnibus, a public functional genomics data repository supporting minimum information about a microarray experiment (MIAME)-compliant data submissions (http://www.ncbi.nlm.nih.gov/geo/).

A $χ^2$ test of homogeneity was carried to test whether the proportion of up- and down-regulated genes was equivalent

across chromosomes. The proportion of misregulated genes was not equivalent across chromosome with posthoc χ^2 analysis using the Marascuilo procedure (Fig. S2).

Electrophysiological Recordings. Whole-cell patch clamp recordings were performed on paired, age-matched populations of Ts21 and control cells after 5–6 wk ($n = 9$ independent paired experiments). Each experiment consisted of 12–20 cells per group (DS2U, DS1, DS4, IMR90, and 2DS3). In all, 469 cells were patched, and >20,000 synaptic events were examined. Cells were superfused with a modified HBSS that contained 140 mM NaCl, 3 mM KCl, 2 mM $CaCl_2$, 1 mM $MgCl_2$, 15 mM Hepes, and 23 mM glucose, pH 7.4, 300 mOsm. All recordings were performed at 21 °C to 23 °C using pipettes with resistances of 3–5 MΩ that were filled with an intracellular recording solution containing 121 mM K-gluconate, 22 mM KCl, 10 mM Na-Hepes, and 10 mM EGTA, pH 7.2, 290 mOsm. Recordings were obtained using a MultiClamp 700B Amplifier (Molecular Devices) filtered at 4 kHz and sampled at 10 kHz using a Digidata 1322A Analog-to-Digital Converter (Molecular Devices). Whole-cell capacitance was fully compensated, and series resistance was compensated >70% except during PSC recordings, where it was not compensated. Access resistance was monitored before and after recordings, and cells with resistances greater than 25 MΩ at either point were discarded from analyses. All data were stored on a computer hard disk and analyzed with Clampfit v9.2 (Molecular Devices). The liquid junction potential was posthoc adjusted according to standard procedures (JPCalc in Clampex; Molecular Devices). PSC analysis was performed using mini analysis software (Synaptosoft). Na^+ and K^+ currents were stimulated using 500-ms voltage steps that varied from −50 to +50 mV in 10-mV increments. Spontaneous action potentials (APs) were measured in current clamp (0 pA); induced APs were generated using current injection steps of +70 pA. Postsynaptic currents were analyzed using MiniAnalysis (Synaptosoft) software. Excitatory postsynaptic current (ePSC) and iPSC discernment was performed using independent applications of 6-cyano-7-nitro-quinoxaline-2,3-dione or picrotoxin (25 μM) to block AMPA or GABA receptors, respectively, on 6-wk-old control neurons. Decay constant (time to decay to half-maximal amplitude) of remaining PSCs after each treatment was determined and used to separate ePSCs (decay constant < 4 ms) and iPSCs (decay constant > 4 ms) automatically using MiniAnalysis. All PSCs were verified visually to ensure accuracy of automated counts. Generally, n values represent three cellular differentiation experiments with two time points (weeks 5 and 6) as independents (Fig. 3). However, for groups where no significant differences were observed between any groups (Fig. S3), data from controls (DS2U and IMR90) and Ts21 lines (DS1, DS4, and 2DS3) were pooled for clarity. Statistical analysis was performed using Student t tests. Data were considered statistically significant a priori if $P < 0.05$.

PCR Primers.

ACTA2 F:CAGGGCTGTTTTCCCATCCAT R:GCCATGT-TCTATCGGGTACTTC

AFP F:AGCTTGGTGGTGGATGAAAC R:CCCTCTTCA-GCAAAGCAGAC

APP F:CTTGGAGAGGTGTGCTCTGAA R:GGTTCCTG-GGTAGTCTTGAGT

β-Actin F:GCGAGAAGATGACCCAGATC R:CCAGTGG-TACGGCCAGAGG

Catalase F:ACTTTGAGGTCACACATGACATT R:CTGA-ACCCGATTCTCCAGCA

c-Myc F:AGGACAGCGGCAGCCCGAAC R:TGGGCGA-GCTGCTGTCGTTG

Crystallin F:ATGGCGACTGGACAGAAGTTG R:GGACC-TTGATTAGAACCTGATGG

Endo c-Myc F:CGGGCGGGCACTTTG R:GGAGAGTCG-CGTCCTTGCT

Endo Klf4 F:AGCCTAAATGATGGTGCTTGGT R:TTGAA-AACTTTGGCTTCCTTGTT

Endo *Oct4* F:AGTTTGTGCCAGGGTTTTTG R:ACTTCA-CCTTCCCTCCAACC

Endo *Sox2* F:CAAAAATGGCCATGCAGGTT R:AGTTG-GGATCGAACAAAAGCTATT

ETS2 F:AACACTGCAAGAAGTGCCAACAGG R:TGTT-CCCAGAGAATGTCACCCACA

Exo cMyc F:GGGTGGACCATCCTCTAGAC R:CCTCGT-CGCAGTAGAAATAC

Exo Klf4 F:GGGTGGACCATCCTCTAGAC R:GGAAGT-CGCTTCATGTGG

Exo *Oct4* F:GGGTGGACCATCCTCTAGAC R:CCAGGT-CCGAGGATCAAC

Exo *Sox2* F:GGGTGGACCATCCTCTAGAC R:GGGCTG-TTTTTCTGGTTG

FoxG1 F:AGAAGAACGGCAAGTACGAGA R: TGTTGA-GGGACAGATTGTGGC

GAPDH F:ACCACAGTCCATGCCATCAC R:TCCACCA-CCCTGTTGCTGTA

Gbx2 F:CTCACCTCTACGCTCATGGC R:CGCCTTGTC-GAAGTTACCG

HoxB4 F:GTGAGCACGGTAAACCCCAAT R:CGAGCG-GATCTTGGTGTTG

Islet1 F:GTTTGAAATGTGCGGAGTGTAAT RTTCTTG-CTGAAGCCGATGC

Klf4 F:TCTCAAGGCACACCTGCGAA R:TAGTGCCTG-GTCAGTTCATC

Lhx2 F:TCGGGACTTGGTTTATCACCT R:GCAAGCCG-CAGTAGACCAG

Nanog F:CAAAGGCAAACAACCCACTT R:TCTGCTGG-AGGCTGAGGTAT

NCAM F:ATGGAAACTCTATTAAAGTGAACCTG R:TA-GACCTCATACTCAGCATTCCAGT

Nkx2.1 F:AGCACACGACTCCGTTCTC R:GCCCACTTT-CTTGTAGCTTTCC

Oct4 F:CGAGCAATTTGCCAAGCTCCTGAA R:TTCGG-GCACTGCAGGAACAAATTC

Otx2 F:AGAGGACGACGTTCACTCG R:TCGGGCAAG-TTGATTTTCAGT

Pax6 F:CGGAGTGAATCAGCTCGGTG R:CCGCTTATA-CTGGGCTATTTTGC

SOD1 F:GCAGGGCATCATCAATTTCGAGCA R:ACAT-TGCCCAAGTCTCCAACATGC

*Sox2* F:CCCCCGGCGGCAATAGCA RTCGGCGCCGGG-GAGATACAT

Tbr1 F:GCCTTTCTCCTTCTATCATGCTC R:GTCAGTG-GTCGAGATAATGGGA

1. Hu BY, et al. (2010) Neural differentiation of human induced pluripotent stem cells follows developmental principles but with variable potency. *Proc Natl Acad Sci USA* 107(9):4335–4340.
2. Hu BY, Zhang SC (2010) Directed differentiation of neural-stem cells and subtype-specific neurons from hESCs. *Methods Mol Biol* 636(2010):123–137.
3. Zhang SC (2006) Neural subtype specification from embryonic stem cells. *Brain Pathol* 16(2):132–142.
4. Zhang SC, Wernig M, Duncan ID, Brüstle O, Thomson JA (2001) In vitro differentiation of transplantable neural precursors from human embryonic stem cells. *Nat Biotechnol* 19(12):1129–1133.
5. Schmittgen TD, Livak KJ (2008) Analyzing real-time PCR data by the comparative C(T) method. *Nat Protoc* 3(6):1101–1108.
6. LaVaute TM, et al. (2009) Regulation of neural specification from human embryonic stem cells by BMP and FGF. *Stem Cells* 27(8):1741–1749.
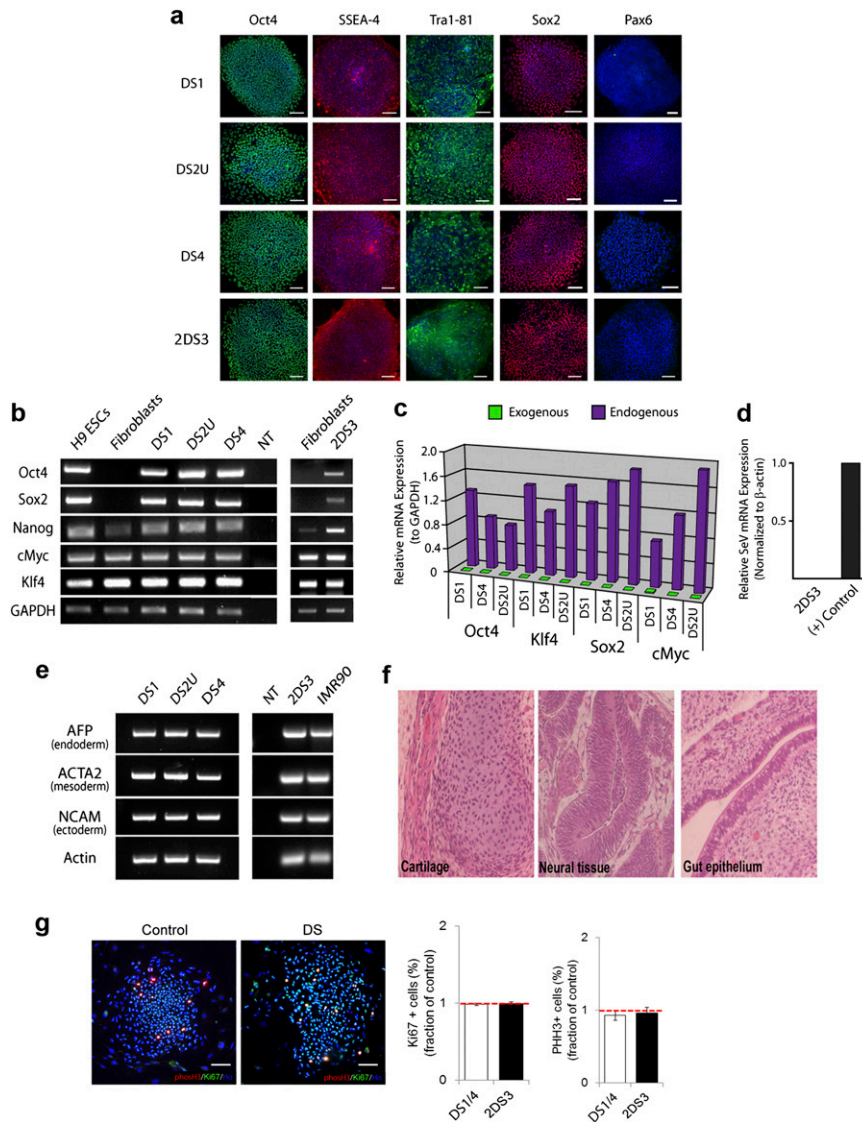
Fig. S1. iPSCs reprogrammed from DS individuals. (*A*) Representative images of iPSCs show expression of pluripotent markers POU class 5 homeobox 1 (*Oct4*) (green), stage-specific embryonic antigen-4 (SSEA-4) (red), Tra 1-81 (green), and SRY-box containing gene 2 (*Sox2*) (red) but not paired box gene 6 (*Pax6*) (green). (Blue) Hoescht. (*B*) iPSC RNA expression signature for pluripotency factors was similar to expression in H9 human embryonic stem cells, whereas parent fibroblasts lacked expression of *Oct4* and *Sox2*. (*C* and *D*) iPSCs down-regulated exogenous and up-regulated endogenous reprogramming factors. (*E*) qPCR analysis revealed expression of markers of all three germ layers in day 30 embryoid bodies. (*F*) H&E staining of sections of teratomas formed by one iPSC line reveals tissue formation of all three germ layers (cartilage, mesoderm; neural tissue, ectoderm; gut epithelium, endoderm). (*G*) Fluorescent images of control and DS iPSC colonies labeled for the cell cycle marker Ki67 (green) and the M-phase marker phospho-histone H3 (PHH3, red). Pooled data revealed no significant difference in either Ki67 or PHH3 proportion between iPSC lines. Error bars are SEM. (Scale bars: 50 μm.)
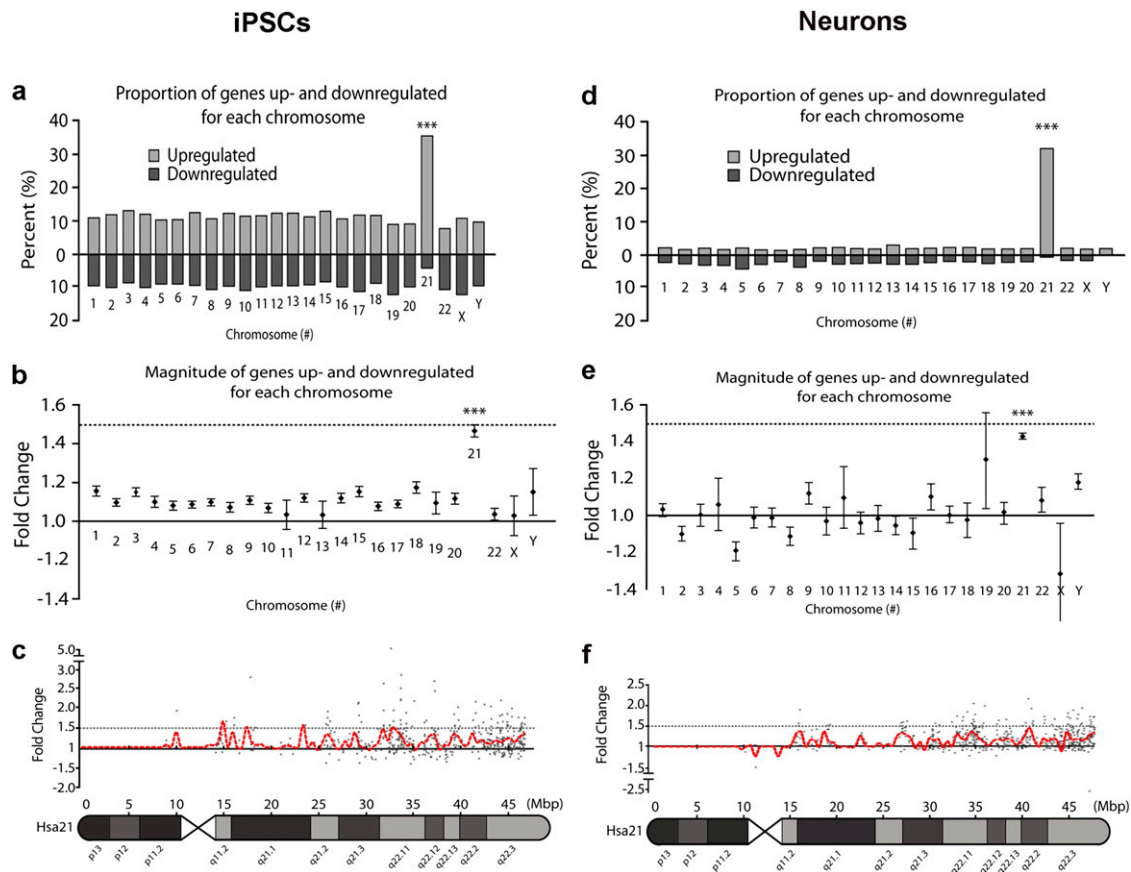
Fig. S2. Gene expression changes throughout the genome in DS iPSCs and neurons. (*A*) Graph depicting the proportion of genes that were up- and down-regulated on each chromosome in DS iPSCs (DS1 and DS4) compared with isogenic control iPSCs (DS2U); a significantly larger fraction of genes was up-regulated, whereas significantly fewer genes were down-regulated on human chromosome 21 (HSA21). (*B*) Average magnitude (fold change) of gene expression is significantly greater for genes on HSA21 in DS iPSCs compared with other chromosomes and control cells [$n = 3$; $F(23, 11,211) = 3.69$; $P < 0.001$ for all chromosomes except chromosome Y]. (*C*) Gene expression changes on HSA21 in DS iPSCs depicted graphically over the entire chromosome. (*D*) Graph depicting the proportion of genes that are up- and down-regulated on each chromosome in DS iPSC-derived neurons (DS1 and DS4) compared with isogenic control neurons (DS2U; $n = 3$, $P < 0.001$). (*E*) The average magnitude (fold change) of gene expression is significantly greater for genes on HSA21 in DS iPSC-derived neurons compared with other chromosomes [$n = 3$; $F(23, 1,318) = 3.15$; $P < 0.001$ for all chromosomes except chromosomes 4, 11, and 19]. (*F*) Graphical depiction of genes changed in DS iPSC-derived neurons over HSA21. ***$P < 0.001$.
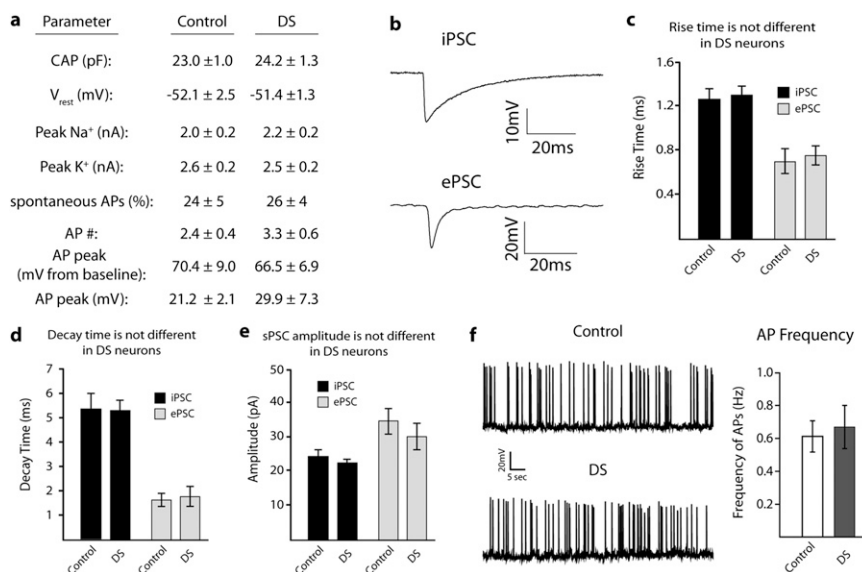
Fig. S3. Physiological properties unaltered in DS iPSC-derived neurons. (*A*) Table of physiological properties that are not significantly different between DS and control cells, including number of APs in response to current injection (AP #; $n = 9$, $P = 0.74$), capacitance (CAP; $n = 9$, $P = 0.94$), resting membrane potential ($n = 9$, $P = 0.48$), and peak AP amplitude ($n = 9$, $P = 0.68$). (*B*) Averaged traces from either (*Upper*) inhibitory (iPSCs) or (*Lower*) excitatory (ePSCs) spontaneous PSCs. (*C–E*) Pooled data show no significant difference in (*C*) rise time, (*D*) decay time, or (*E*) amplitude of either iPSCs or ePSCs in between DS and control neurons after 5–6 wk of differentiation. (*F*) Representative traces from either (*Upper Left*) control or (*Lower Left*) DS iPSC-derived neurons held at endogenous resting membrane potentials that display spiking. Pooled data show no significant difference in AP frequency between DS and control neurons after 5–6 wk of differentiation ($n = 9$, $P = 0.4$). Error bars are SEM.

Table S1. Antibodies

Target	Catalogue no.	Manufacturer	Clonality	Dilution
β-III tubulin	T8660	Sigma	Mouse monoclonal	1:1,000
β-III tubulin	PRB-435P	Covance	Rabbit polyclonal	1:5,000
β-III tubulin	AB9354	Millipore	Chicken polyclonal	1:3,000
FoxG1	ab18259	Abcam	Rabbit polyclonal	1:100
GABA	A2052	Sigma	Rabbit polyclonal	1:1,000
Oct4	SC-5279	Santa Cruz	Mouse monoclonal	1:500
Otx2	AF1979	R&D	Goat polyclonal	1:500
Pax6	PRB-278P	Covance	Rabbit polyclonal	1:300
Sox2	MAB2018	R&D	Mouse monoclonal	1:1,000
SSEA4	MAB4304	Millipore	Mouse monoclonal	1:1,000
Synapsin	574777	Calbiochem	Rabbit polyclonal	1:1,000
Synapsin	106-001	Synaptic Systems	Mouse monoclonal	1:1,000
Tra1-81	MAB4381	Millipore	Mouse monoclonal	1:500
VGAT	131-011	Synaptic Systems	Mouse monoclonal	1:1,000

Other Supporting Information Files

Dataset S1 (XLSX)
Dataset S2 (XLSX)
Dataset S3 (XLSX)
Dataset S4 (XLSX)